arXiv:0902.3284v1 [nucl-th] 19 Feb 2009

Constraining the EOS of neutron-rich nuclear matter and properties of neutron stars with heavy-ion reactions

Bao-An Li*, Lie-Wen Chen†, Che Ming Ko**, Plamen G. Krastev*,‡, De-Hua Wen*,§, Aaron Worley*, Zhigang Xiao¶, Jun Xu†,**, Gao-Chan Yong$^{*,\|}$ and Ming Zhang¶

**Department of Physics, Texas A&M University-Commerce, Commerce, Texas 75429-3011, USA*
†*Institute of Theoretical Physics, Shanghai Jiao Tong University, Shanghai 200240, China*
***Cyclotron Institute and Physics Department, Texas A&M University, College Station, Texas 77843-3366, USA*
‡*Department of Physics, San Diego State University, 5500 Campanile Drive, San Diego CA 92182-1233, USA*
§*Department of Physics, South China University of Technology, Guangzhou 510641, China*
¶*Department of Physics, Tsinghua University, Beijing 100084, China*
$^\|$*Institute of Modern Physics, Chinese Academy of Sciences, Lanzhou 730000, China*

Abstract. Heavy-ion reactions especially those induced by radioactive beams provide useful information about the density dependence of the nuclear symmetry energy, thus the Equation of State of neutron-rich nuclear matter, relevant for many astrophysical studies. The latest developments in constraining the symmetry energy at both sub- and supra-saturation densities from analyses of the isopsin diffusion and the π^-/π^+ ratio in heavy-ion collisions using the IBUU04 transport model are discussed. Astrophysical ramifications of the partially constrained symmetry energy on properties of neutron star crusts, gravitational waves emitted by deformed pulsars and the w-mode oscillations of neutron stars are presented briefly.

Keywords: Equation of State, neutron-rich matter, nuclear symmetry energy, heavy-ion reactions, neutron stars, gravitational waves
PACS: 21.65.Cd, 21.65.Ef, 25.70.-z, 21.30.Fe,21.10.Gv, 26.60-c.

CONSTRAINING THE DENSITY DEPENDENCE OF NUCLEAR SYMMETRY ENERGY WITH HEAVY-ION COLLISIONS

To determine the density dependence of the nuclear symmetry energy $E_{sym}(\rho)$, thus the equation of state (EOS) of neutron-rich nuclear matter, has been a longstanding goal of both nuclear physics and astrophysics. The $E_{sym}(\rho)$ is critical for understanding not only the structure of rare isotopes and heavy-ion reactions [1, 2, 3, 4, 5], but also many interesting issues in astrophysics [6, 7, 8, 9]. In this contribution we first summarize some recent progress in constraining the $E_{sym}(\rho)$ from analyzing the isospin diffusion and π^-/π^+ ratio in heavy-ion collisions within an isospin and momentum dependent transport model IBUU04 [10]. We will then discuss some astrophysical ramifications of the partially constrained $E_{sym}(\rho)$. Some interesting information about the $E_{sym}(\rho)$ has been obtained over the last few years from heavy-ion collisions [5]. As an example, shown in the middle of Fig. 1 are the $E_{sym}(\rho)$ used in the IBUU04 transport model. The three MDI $E_{sym}(\rho)$ [11] are obtained using a modified Gogny force by adjusting the parameter x introduced in the interaction. For comparisons, the IQMD [12] and the APR[13] predictions are also shown. Shown in the left window is the degree of isospin diffusion $1-R_i$ [14, 15, 16] versus the slope parameter $L \equiv 3\rho_0 \frac{\partial E_{\rm sym}(\rho)}{\partial \rho}|_{\rho=\rho_0}$ of the MDI symmetry energy. Within the IBUU04 model analysis, the MSU data of Tsang et al. [14] favors a $E_{sym}(\rho)$ between that with $x=0$ and $x=-1$ around the APR prediction. More quantitatively, one can infer that the slope parameter is about $L = 88 \pm 25$ MeV [17]. We notice that a very recent re-analysis of the MSU isospin diffusion data using the ImQMD model found that the extracted range of the $E_{sym}(\rho)$ overlaps with that from the IBUU04 analysis around the $E_{sym}(\rho)$ with $x=0$ (or APR) [18]. In the MSU isospin diffusion reactions the maximum density reached is about $1.2\rho_0$ [15]. Moreover, the isospin diffusion was found to probe the symmetry energy during the expansion phase of the reaction [14, 15]. Thus the isospin diffusion data provides us information about the $E_{sym}(\rho)$ in the sub-saturation density region.

Very interestingly, a recent IBUU04 transport model analysis of the FOPI/GSI π^-/π^+ ratio data [20] in relativistic heavy-ion collisions at SIS/GSI with beam energies above 400 MeV/A provides circumstantial evidence suggesting a rather soft nuclear symmetry energy at $\rho \geq 2\rho_0$ compared to the APR prediction [19]. Shown in the right window are the calculated π^-/π^+ ratios in comparison with the FOPI data at 0.4 AGeV with the reduced impact parameter

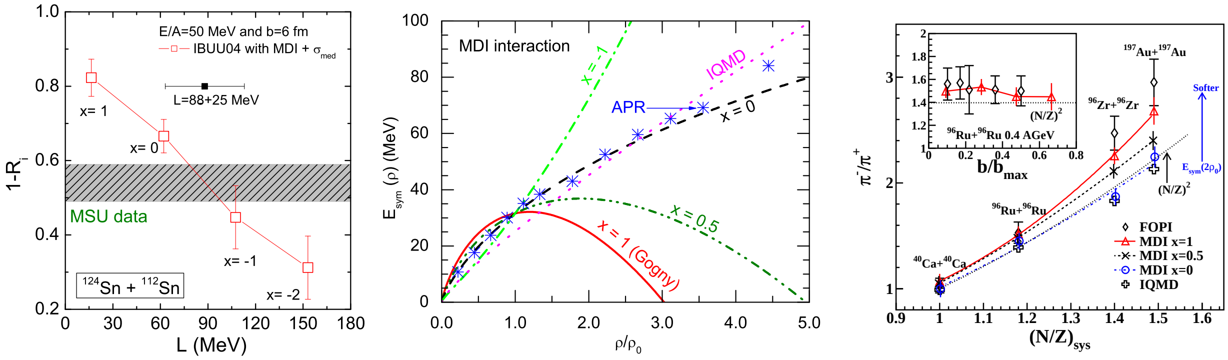

FIGURE 1. Left: Degree of the isospin diffusion $1-R_i$ as a function of the slope parameter L of the symmetry energy. Middle: The density dependence of the symmetry energy. Right: The π^-/π^+ ratio as a function of the neutron/proton ratio of the reaction system at 0.4 AGeV with the reduced impact parameter of $b/b_{max} \leq 0.15$. The inset is the impact parameter dependence of the π^-/π^+ ratio for the ^{96}Ru+^{96}Ru reaction at 0.4 AGeV. Taken from Refs. [17, 19].

$b_0 \equiv b/b_{max} \leq 0.15$ as a function of the neutron/proton ratio of the reaction system. The inset shows the π^-/π^+ ratio as a function of b_0 for the ^{96}Ru+^{96}Ru reaction at 0.4 AGeV. It is seen that both the data and the calculations exhibit very weak b_0 dependence for the π^-/π^+ ratio, even for mid-central reactions where we found that the multiplicities of both π^- and π^+ vary appreciably with the b_0. For the symmetric ^{40}Ca+^{40}Ca and the slightly asymmetric ^{96}Ru+^{96}Ru reactions, calculations using both $x=1$ and $x=0$ can well reproduce the FOPI data. Most interestingly, for the more neutron-rich reactions of ^{96}Zr+^{96}Zr and ^{197}Au+^{197}Au calculations with $x=0, 0.5$ and 1 are clearly separated from each other. The FOPI data favors clearly the calculation with $x=1$. The corresponding symmetry energy is much softer than the APR prediction. A detailed study on the excitation function of the π^-/π^+ ratio also indicates that the FOPI data can be approximately reproduced only with the $x=1$ symmetry energy [19]. It is also interesting to mention that IQMD calculations [20] give similar results as the IBUU04 with $x=0$. This is not surprising since the symmetry energy functionals used in the IQMD and the IBUU04 with x=0 are very similar for $\rho_0 < \rho \leq 3\rho_0$ as shown in the middle of Fig. 1. The most importance influence of a rather soft symmetry energy at supra-saturation densities, such as that with $x=1$, on pion production is through the rather high neutron/proton ratio reached in the participant region due to the dynamical isospin fractionation. As shown in the middle window, with $x=1$ the $E_{sym}(\rho)$ at $\rho \geq 2\rho_0$ reached in the reaction is very small. Thus a rather high N/Z in the participant region is energetically favored due to the dynamical isospin fractionation [21, 22] and thus the larger π^-/π^+ ratio is observed. In the reactions considered at 400 MeV/A, the maximum central density reached is about $2.5\rho_0$. By varying separately the $E_{sym}(\rho)$ at sub- and supra-saturation densities used in the IBUU04 simulations for these reactions it was found that the π^-/π^+ ratio is much more sensitive to the variation of the $E_{sym}(\rho)$ at supra-saturation rather than sub-saturation densities.

Putting together the information from analyzing both the isospin diffusion and the π^-/π^+ ratio data, we expect that the $E_{sym}(\rho)$ reaches a maximum somewhere between ρ_0 and $2\rho_0$ before it starts decreasing at higher densities. This indicates the importance of mapping out the $E_{sym}(\rho)$ at densities from about ρ_0 to $2.5\rho_0$. Such experiments are being planned at several facilities. If the $E_{sym}(\rho)$ is confirmed by more experimental and theoretical studies to decrease with increasing density above certain density, it not only posts a serious challenge to some nuclear many-body theories but also has important implications on several critical issues in nuclear astrophysics, such as, the cooling of proto-neutron stars, the possible formation of polarons due to the isospin separation instability [23, 24], the possible formation of quark droplets [25] and hyperons [26] in the core of neutron stars.

Since the $E_{sym}(\rho)$ is only partially constrained in some density regions by the available experimental data within the IBUU04 transport model analyses, astrophysical applications of these constraints involve some interpolations and/or extrapolations under some assumptions. We notice here, however, that the extrapolation of any low-density symmetry energy to supra-saturation densities can be very dangerous as illustrated in Fig. 1. Using the same IBUU04 transport model, at sub-saturation densities the isospin diffusion analyses favors clearly the APR prediction, but above about $2\rho_0$ the π^-/π^+ ratio data favors instead the Gogny prediction that is much softer than the APR prediction. Fortunately, while many astrophysical questions depend on the symmetry energy over the whole density range, some issues, such as the core-crust transition density in neutron stars depends only on the $E_{sym}(\rho)$ at sub-saturation densities. In the following section, we present several examples illustrating the astrophysical importance of the $E_{sym}(\rho)$ using the MDI

EOS with $x = 0$ and $x = -1$ extrapolated to supra-saturation densities. Effects of the softening of the $E_{sym}(\rho)$, such as that with $x = 1$, is currently under investigation.

NUCLEAR CONSTRAINTS ON PROPERTIES OF NEUTRON STAR CRUSTS

Neutron stars are expected to have a solid inner crust surrounding a liquid core. Knowledge on properties of the crust plays an important role in understanding many astrophysical observations [6, 7, 8, 9, 27, 28, 29, 30, 31, 32, 33, 34]. The inner crust spans the region from the neutron drip-out point to the inner edge separating the solid crust from the homogeneous liquid core. While the neutron drip-out density ρ_{out} is relatively well determined to be about 4×10^{11} g/cm^3 [35], the transition density ρ_t at the inner edge is still largely uncertain mainly because of our very limited knowledge on the EOS, especially the density dependence of the symmetry energy, of neutron-rich nucleonic matter [6, 8]. Recently, using the equation of state for neutron-rich nuclear matter constrained by the isospin diffusion data from heavy-ion reactions in the same sub-saturation density range as the neutron star crust, Xu et al. put a tight constraint on the location of the inner edge of neutron star crusts [36].

The density and pressure at the core-crust transition

The inner edge corresponds to the phase transition from the homogeneous matter at high densities to the inhomogeneous matter at low densities. In principle, the inner edge can be located by comparing in detail relevant properties of the nonuniform solid crust and the uniform liquid core mainly consisting of neutrons, protons and electrons (*npe* matter). However, this is practically very difficult since the inner crust may contain nuclei having very complicated geometries, usually known as the 'nuclear pasta' [7, 32, 37, 38, 39]. Furthermore, the core-crust transition is thought to be a very weak first-order phase transition and model calculations lead to very small density discontinuities at the transition [30, 40, 41, 42]. In practice, therefore, a good approximation is to search for the density at which the uniform liquid first becomes unstable against small amplitude density fluctuations with clusterization. This approximation has been shown to produce very small error for the actual core-crust transition density and it would yield the exact transition density for a second-order phase transition [30, 40, 41, 42]. Several such methods including the dynamical method [27, 28, 29, 30, 40, 43, 44], the thermodynamical method [8, 45, 46] and the random phase approximation (RPA) [42, 47] have been applied extensively in the literature.

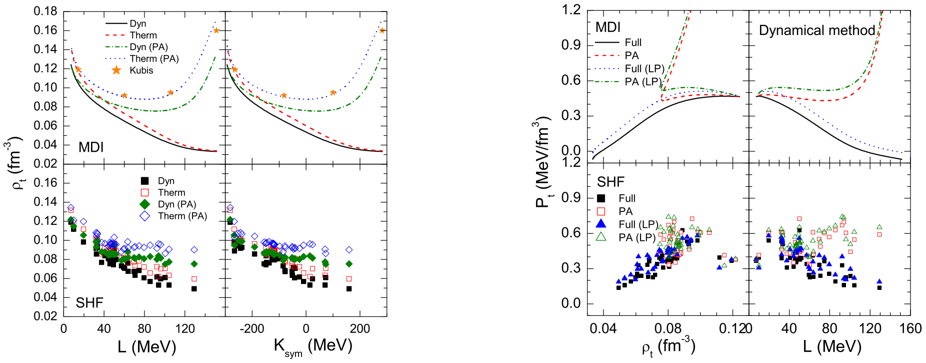

FIGURE 2. Left: The transition density ρ_t as a function of L (left windows) and K_{sym} (right windows) by using both the dynamical and thermodynamical methods with the full EOS and its parabolic approximation. Right: The transition pressure P_t as a function of ρ_t and L within the dynamical method with the full EOS and its parabolic approximation. The MDI (upper windows) and Skyrme interactions (lower windows) are used. Taken from Ref. [36].

Shown in the left panel of Fig. 2 is the ρ_t as a function of L and $K_{sym} \equiv 9\rho_0^2 \frac{\partial^2 E_{sym}(\rho)}{\partial \rho^2}|_{\rho=\rho_0}$ using both the dynamical and thermodynamical methods with the full EOS and its parabolic approximation (PA) from the MDI interaction with the varying x parameter and 47 Skyrme forces [36]. With the full MDI EOS, it is clearly seen that the ρ_t decreases almost linearly with increasing L for both methods. This feature is consistent with the RPA results [47] and that found recently by Oyamatsu et al. [43]. The similar relation is also observed between the ρ_t and K_{sym} due to the fact that K_{sym} always correlate with L for a fixed energy density functional [36]. It is interesting to see that both the dynamical

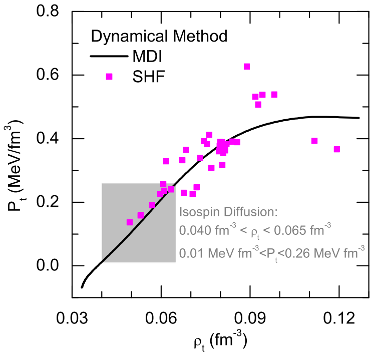

FIGURE 3. P_t as a function of ρ_t by using the dynamical method without parabolic approximation for both MDI interaction and SHF calculations. The shaded band represent the constraint from the isospin diffusion data. Taken from Ref. [36].

and thermodynamical methods give very similar results. On the other hand, surprisingly, the PA drastically changes the results, especially for stiffer symmetry energies (larger L values). Also included in the left panel of Fig. 2 are the predictions by Kubis using the PA of the MDI EOS in the thermodynamical approach [45]. The large error introduced by the PA is understandable since the β-stable npe matter is usually highly neutron-rich and the contribution from the higher order terms in δ is appreciable. This is especially the case for the stiffer symmetry energy which generally leads to a more neutron-rich npe matter at subsaturation densities. In addition, simply because of the energy curvatures involved in the stability conditions, the contributions from higher order terms in the EOS are multiplied by a larger factor than the quadratic term. These features agree with the early finding [48] that the ρ_t is very sensitive to the fine details of the nuclear EOS. Applying the experimentally constrained L values of 86 ± 25 MeV to the $\rho_t - L$ correlation obtained using the full EOS within the dynamical method shown in the left panel of Fig. 2, one can conclude that the transition density is between 0.040 fm^{-3} and 0.065 fm^{-3}. This constrained range is significantly below the fiducial value of $\rho_t \approx 0.08$ fm^{-3} often used in the literature and the estimate of $0.5 < \rho_t/\rho_0 < 0.7$ made in ref. [8] within the thermodynamical approach using the parabolic approximation of the EOS.

The pressure at the inner edge is an important quantity related directly with the crustal fraction of the moment of inertia which can be measurable indirectly from observations of pulsar glitches [8]. It is very instructive to quote the analytical estimation obtained by Lattimer and Prakash [8] for the transition pressure

$$P_t = \frac{K_0}{9}\frac{\rho_t^2}{\rho_0}\left(\frac{\rho_t}{\rho_0}-1\right)+\rho_t\delta_t\left[\frac{1-\delta_t}{2}E_{sym}(\rho_t)+\left(\rho\frac{dE_{sym}(\rho)}{d\rho}\right)_{\rho_t}\delta_t\right], \tag{1}$$

where K_0 is the incompressibility of symmetric nuclear matter at ρ_0 and δ_t is the isospin asymmetry at ρ_t. One can see that, besides the implicit dependence on the symmetry energy through the ρ_t and δ_t, the P_t also depends explicitly on the value and slope of the $E_{sym}(\rho)$ at ρ_t. Thus the P_t depends very sensitively on the $E_{sym}(\rho)$. Shown in the right panel of Fig. 2 is the P_t as a function of ρ_t (left windows) and L (right windows) by using the dynamical method with and without the parabolic approximation. The results from Eq. (1) using the ρ_t and E_{sym} corresponding to the full EOS and its PA are also shown for comparisons. It is interesting to see that the Eq. (1) predicts qualitatively the same but quantitatively slightly higher values compared to the original expressions for the pressure with or without the PA for both the thermodynamical and dynamical methods even though this formula was derived from the thermodynamical method using the PA. This observation implies that the direct effect of using the full EOS or its PA on the pressure is small although the PA may affect strongly the transition pressure P_t by changing the transition density ρ_t. The P_t essentially increases with the increasing ρ_t in calculations using the full EOS, but a complex relation between the P_t and ρ_t is obtained using the PA. The large difference in P_t is due to the strong PA effect on the ρ_t. Moreover, the latter does not vary monotonically with L for the PA as shown in the right panel of Fig. 2.

It is also interesting to examine the range of P_t corresponding to the ρ_t and L constrained by the heavy-ion reaction data. In Fig. 3, we show the P_t as a function of ρ_t by using the dynamical method and the full EOS for both the MDI (solid line) and the Skyrme (filled squares) calculations. It is interesting to see that the MDI and Skyrme interactions give generally quite consistent results. Corresponding to the ρ_t constrained in between 0.040 fm^{-3} and 0.065 fm^{-3}, the P_t is limited between 0.01 MeV/fm^3 and 0.26 MeV/fm^3 with the MDI interaction as indicated by the shaded area,

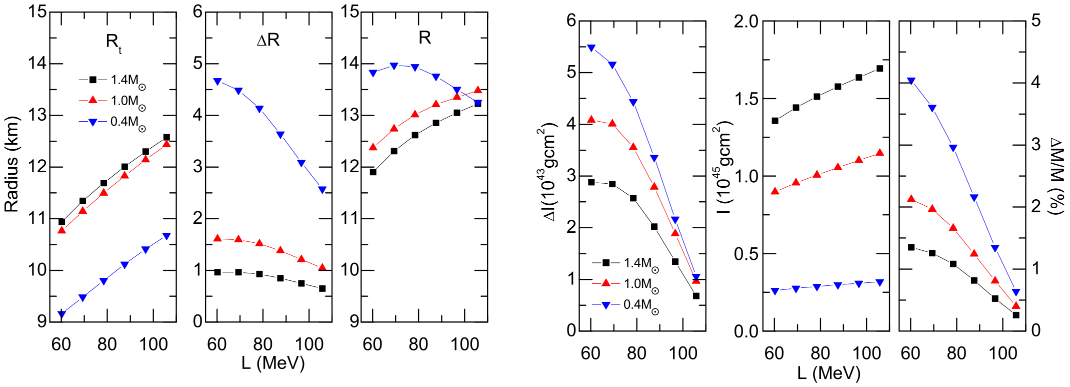

FIGURE 4. Left: The whole radius R, the crust thickness ΔR, the core radius R_t as functions of L at fixed total mass of $0.4M_\odot$, $1.0M_\odot$ and $1.4M_\odot$, respectively. Right: The crustal fraction of neutron mass $\Delta M/M$, the moment of inertia I of the whole star and the crust contribution ΔI as a function of L, at fixed total mass $0.4M_\odot$, $1.0M_\odot$ and $1.4M_\odot$, respectively. Taken from Ref. [36].

which is significantly less than the fiducial value of $P_t \approx 0.65$ MeV/fm^3 often used in the literature [8]. As pointed out in a recent work by Avancini et al [49], the value of $P_t \approx 0.65$ MeV/fm^3 may be too large for most mean-field calculations without the PA. We note that among the 47 Skyrme interactions used here, the following 8 interactions, i.e., the SkMP, SKO, R$_\sigma$, G$_\sigma$, SV, SkI2, SkI3, and SkI5, are consistent with the constraints from heavy-ion reactions. These results indicate that one may introduce a huge error by assuming *a priori* that the EOS is parabolic for a given interaction in calculating the ρ_t and P_t.

The core size and crust thickness

For a given neutron star of total mass M and radius R, what are the respective sizes of its core and crust? How do they depend on the stiffness of the symmetry energy? How do they depend on the neutron star mass M? How does the thickness of neutron star crusts depend on L while it is well known that the size of neutron skin in heavy nuclei increases with the increasing L [17]? These questions have been investigated recently in Ref. [36].

Show in left panel of Fig. 4 are the core radius R_t, the crust thickness ΔR and the total radius R as functions of L for a fixed total mass of $0.4M_\odot$, $1.0M_\odot$ and $1.4M_\odot$, respectively. It is seen that the R_t increases almost linearly with increasing L. The R_t also increases with the increasing mass at a fixed L. This is because the stiffer the symmetry energy is, the larger the contribution of the isospin asymmetric part of the pressure will be, which makes the R_t larger. Moreover, the ΔR decreases with the increasing L especially for light neutron stars, as the transition density decreases with the increasing L. As the thickness of the crust ΔR and the core radius R_t depend oppositely on L, the total radius $R = R_t + \Delta R$ of the neutron star may show a complicated dependence on L. We stress here that this is the result of a competition between the repulsive nuclear pressure dominated by the symmetry energy contribution and the gravitational binding. Interestingly, it is often mentioned that the crust of neutron stars bears some analogy with the neutron-skin of heavy nuclei. However, they show completely opposite dependences on the L. Namely, the size of neutron-skin usually increases with the increasing L as a result of the competition between the nuclear surface tension and the pressure difference of neutrons and protons [17], while the thickness of neutron star crusts decreases with the increasing L as a result of the competition between the nuclear pressure and the gravitational binding.

The fractional mass and momenta of inertia of neutron star crust

What is the crustal fraction $\Delta M/M$ of the total mass and how does it depend on the symmetry energy? Since the mass is simply the integration of the energy density, one expects the $\Delta M/M$ and $\Delta R/R$ have very similar dependences on L [36]. Shown in the right window of Fig. 4 (right panel) is the $\Delta M/M$. The fractional mass of the crust decreases with the increasing L at a fixed total mass, and it decreases with the increasing total mass at a fixed value of L. The moment of inertia is determined by the distribution of the energy density. From the middle window, it is seen that the total moment of inertia increases with the increasing mass at a fixed value of L and increases with the increasing L at a fixed total mass. The dependence on L is relatively weak especially for light neutron stars. However, the crust contribution of the moment of inertia varies much more quickly with L. It decreases with the increasing neutron star mass at a fixed value of L and decreases with the increasing L at a fixed total mass. These are all consistent with the behaviors of the fractional mass and size of the crust.

The crustal fraction of the moment of inertia $\Delta I/I$ is particularly interesting as it can be inferred from observations of pulsar glitches, the occasional disruptions of the otherwise extremely regular pulsations from magnetized, rotating neutron stars. It can be expressed approximately as [8, 6]

$$\frac{\Delta I}{I} \quad = \quad \frac{28\pi P_t R^3}{3Mc^2}\frac{(1-1.67\xi-0.6\xi^2)}{\xi}\left[1+\frac{2P_t(1+5\xi-14\xi^2)}{\rho_t mc^2\xi^2}\right]^{-1}, \tag{2}$$

where m is the mass of baryons and $\xi = GM/Rc^2$. This analytical formula has been verified by direct numerical calculations using both the full EOS and its PA [36]. Furthermore, it is indicated that there exists big differences for $\Delta I/I$ by comparing calculations using the full EOS and its PA [36], again due to the corresponding differences in the transition density. As it was stressed in ref. [6], the $\Delta I/I$ depends sensitively on the symmetry energy at sub-saturation densities through the P_t and ρ_t, but there is no explicit dependence upon the EOS at higher-densities. Experimentally, the crustal fraction of the moment of inertia has been constrained as $\Delta I/I > 0.014$ from studying the glitches of the Vela pulsar [31]. Combining the observational constraint of $\Delta I/I > 0.014$ with the upper bounds of $\rho_t = 0.065$ fm^{-3} and $P_t = 0.26$ MeV/fm^3 inferred from heavy-ion reactions, we can obtain a minimum radius of $R \geq 4.7 + 4.0M/M_\odot$ km for the Vela pulsar. According to this constraint, the radius of the Vela pulsar is predicted to exceed 10.5 km should it have a mass of $1.4M_\odot$. We notice that a constraint of $R \geq 3.6 + 3.9M/M_\odot$ km for this pulsar has previously been derived in Ref. [31] by using $\rho_t = 0.075$ fm^{-3} and $P_t = 0.65$ MeV/fm^3. However, the constraint obtained here using data from both the terrestrial laboratory experiments and astrophysical observations is significantly different and actually it is more stringent.

IMPRINTS OF SYMMETRY ENERGY ON GRAVITATION WAVES

Gravitational waves are tiny disturbances in space-time and are a fundamental, although not yet directly confirmed, prediction of General Relativity. They can be triggered in cataclysmic events involving (compact) stars and/or black holes. They could even have been produced during the very early Universe, well before any stars had been formed, merely as a consequence of the dynamics and expansion of the Universe. Because gravity interacts extremely weakly with matter, gravitational waves would carry a genuine picture of their sources and thus provide undisturbed information that no other messenger can deliver [50]. Gravitational wave astrophysics would open an entirely new non-electromagnetic window making it possible to probe physics that is hidden or dark to current electromagnetic observations [51].

Deformed pulsars and various oscillation modes of spherical neutron stars are among the possible sources of gravitational waves. In particular, the deformed pulsars are major candidates for sources of continuous gravitational waves in the frequency bandwidth of the existing ground-based laser interferometric detectors including the LIGO [52] and VIRGO (e.g. Ref. [53]). While the oscillations of neutron stars are mostly at frequencies much higher than the currently existing and planned gravitational wave observatories, their studies are of fundamental theoretical interest. The strain-amplitude of gravitational waves from deformed pulsars depends on the star's quadrupole moment determined by the EOS of neutron-rich nuclear matter. On the other hand, both the frequency and the decay rate of the fundamental oscillation modes are determined also by the EOS of neutron-rich nuclear matter. In the following we present several examples illustrating the imprints of the symmetry energy on gravitation waves. More details can by found in refs. [54, 55, 56].

Gravitational waves from deformed pulsars

The strain amplitude of gravitational waves at the Earth's vicinity (assuming an optimal orientation of the rotation axis with respect to the observer) from deformed pulsars can be written as [58]

$$h_0 = \frac{16\pi^2 G}{c^4}\frac{\varepsilon I_{zz}\nu^2}{r}, \tag{3}$$

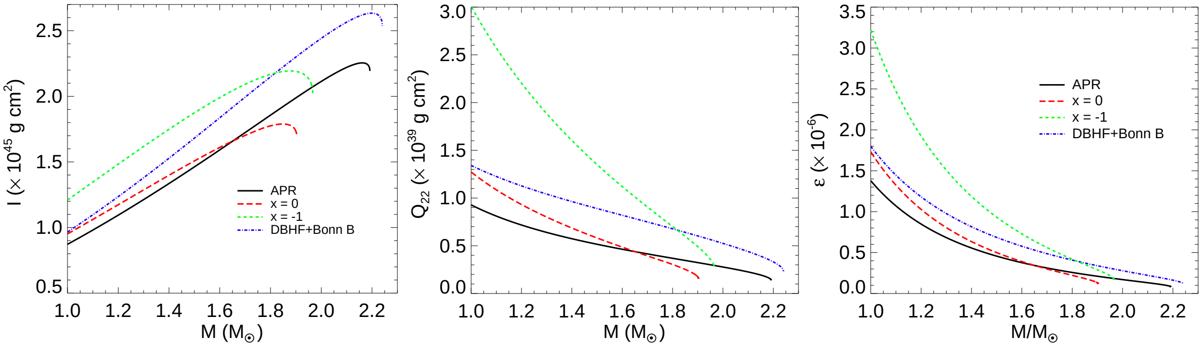

FIGURE 5. Neutron star moment of inertia (left), quadrupole moment (middle) and ellipticity (right) as functions of the neutron star mass. Taken from Ref. [54, 57]

where ν is the neutron star rotational frequency, I_{zz} its principal moment of inertia, $\varepsilon = (I_{xx} - I_{yy})/I_{zz}$ its equatorial ellipticity, and r its distance to Earth. The ellipticity is related to the neutron star maximum quadrupole moment (with $m = 2$) via [59]

$$\varepsilon = \sqrt{\frac{8\pi}{15}} \frac{\Phi_{22}}{I_{zz}}, \tag{4}$$

where for *slowly* rotating (and static) neutron stars Φ_{22} can be written as [59]

$$\Phi_{22,max} = 2.4 \times 10^{38} g\ cm^2 \left(\frac{\sigma}{10^{-2}}\right) \left(\frac{R}{10km}\right)^{6.26} \left(\frac{1.4M_\odot}{M}\right)^{1.2} \tag{5}$$

In the above expression σ is the breaking strain of the neutron star crust which is rather uncertain at present time and lies in the range $\sigma = [10^{-5} - 10^{-2}]$ [58]. From Eqs. (3) and (4) it is clear that h_0 does not depend on the moment of inertia I_{zz}, and that the total dependence upon the EOS is carried by the quadrupole moment Φ_{22}. Thus Eq. (3) can be rewritten as

$$h_0 = \chi \frac{\Phi_{22} \nu^2}{r}, \tag{6}$$

with $\chi = \sqrt{2045\pi^5/15} G/c^4$. For slowly rotating neutron stars Lattimer and Schutz [60] derived the following empirical relation for the moment of inertia

$$I \approx (0.237 \pm 0.008) MR^2 \left[1 + 4.2 \frac{Mkm}{M_\odot R} + 90 \left(\frac{Mkm}{M_\odot R}\right)^4\right] \tag{7}$$

Using Eq. (7) to calculate the neutron star moment of inertia and Eq. (5) the corresponding quadrupole moment, the ellipticity ε can be readily computed (via Eq. (4)). The results are shown in Fig. 5. It is clearly seen that the EOS, especially the symmetry energy, has a strong effects on all of these important quantities.

Since the global properties of spinning neutron stars (in particular the moment of inertia) remain approximately constant for rotating configurations at frequencies up to $\sim 300 Hz$ [46], the above formalism can be readily employed to estimate the gravitational wave strain amplitude, provided one knows the exact rotational frequency and distance to Earth, and that the frequency is relatively low (below $\sim 300 Hz$).

Shown in the left window of Fig. 6 is the GW strain amplitude, h_0, as a function of frequency for several slowly rotating near-earth neutron stars. At higher rotational frequencies, relativistic rotational models have to be used [55]. The solid line represents the designed upper detection limit of LIGO. Shown in the right window is the h_0 for the PSR J1748-2446 rotating at 716z assuming it has an ellipticity of $\varepsilon = 10^{-6}$. In both cases clear imprints of the symmetry energy are seen.

Gravitational waves from the axial w-mode oscillations of neutron stars

In the framework of general relativity, gravitational radiation damps out the neutron star oscillations which leads to the frequency of the non-radial oscillations to become "quasi-normal" (complex) with a real part representing

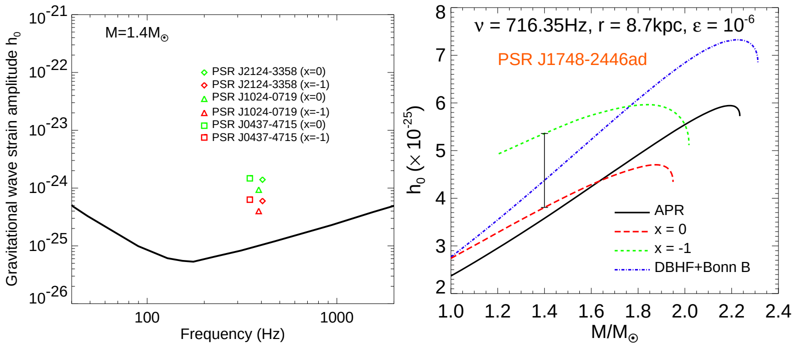

FIGURE 6. Gravitational-wave strain amplitude as a function of frequency for several slow pulsars (left) and PSR J1748-2446 (right). Taken from Ref. [54, 55]

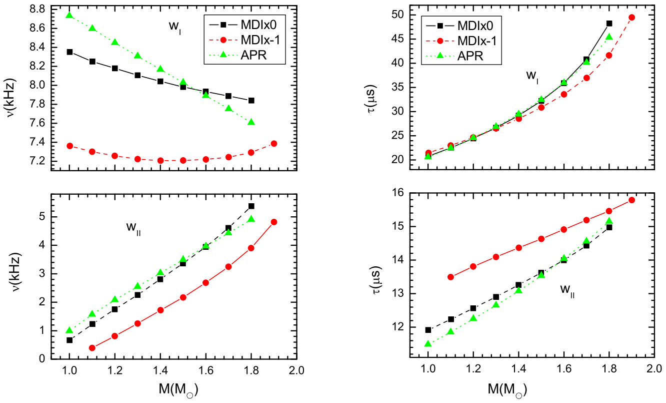

FIGURE 7. Frequency (left) and decay time (right) of w_I-mode (upper) and w_{II}-modes (lower) as functions of the neutron star mass M. Taken from ref. [56]

the actual frequency of the oscillation and an imaginary part representing the losses due to its damping [61]. The eigen-frequencies of the quasi-normal modes could be found by solving the equations which describe the non-radial perturbations of a static neutron star in general relativity. The critical input to solve the equation is the nuclear EOS. The so called w-mode associated with the space-time perturbation only exists in general relativity. It is very important for astrophysical applications since it is related to the space-time curvature and exists for all relativistic stars, including black holes. Using the MDI EOS, Wen et al. recently studied the axial w-modes [56]. Figure 7 displays both the frequency and damping time of the w_I- (upper frame) and w_{II}-modes (lower frame) respectively, as a function of the neutron star mass. The results establish the relationship between the expected frequencies of the axial w-modes, for a given EOS, and the stellar mass. It is interesting to notice that there is a clear difference between the frequencies calculated with the MDI ($x = 0$) EOS and those with the MDI ($x = -1$) EOS. Since the major difference between these two cases is the density dependence of the nuclear symmetry energy, it is obvious that the symmetry energy has a clear imprint on the frequencies.

Shown in Fig. 8 are the real (upper panel) and imaginary (lower panel) parts of the eigen-frequency of w_I and w_{II}-modes scaled by the mass M as a function of the compactness parameter M/R, respectively. These results suggest that the scaled eigen-frequency exhibits a universal behavior as a function of the compactness parameter independent of the EOS used. As discussed by Andersson [62], Benhar [63] and Tsui [64] this finding could be used to constrain the frequency and damping time of gravitational waves. This is very important for guiding the gravitational wave search provided the mass and radius of the prospective source (neutron star) are known. On the other hand, when the gravitational wave astronomy becomes a reality, namely if both the frequency and dumping time for a given neutron star are known this could provide information on the neutron star mass and radius. In Figs. 8 the fitting curves

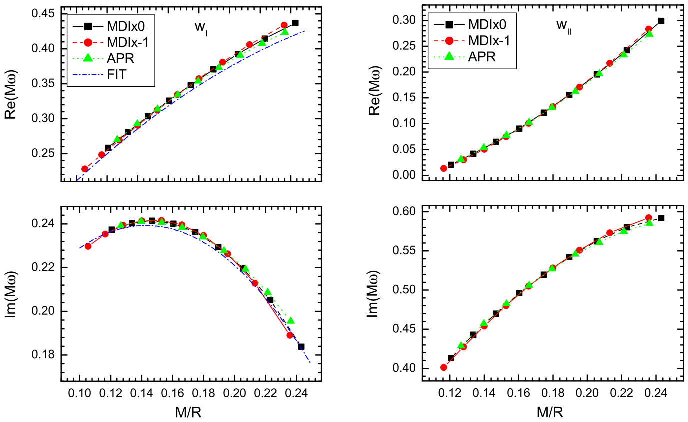

FIGURE 8. The scaled frequency (left) and decay time (right) of w_I-mode (upper) and w_{II}-modes (lower) as functions of the neutron star compactness M/R. Taken from ref. [56]

representing the results of Tsui et al. [64] are also shown. It is seen that the numerical results of Wen et al. are in good agreement with those of Tsui et al. [64].

SUMMARY

In summary, important progress has been made in recent years in constraining the symmetry energy with heavy-ion collisions. Their implications in some astrophysical phenomena have been explored. Nevertheless, the field is still at its beginning. While a number of potentially useful probes of the $E_{sym}(\rho)$ have been proposed, available experimental data are mostly for reactions with stable beams [5]. Coming experiments with more neutron-rich nuclei at several advanced radioactive beam facilities are expected to improve the situation dramatically. Thus, more exciting times are yet to come.

ACKNOWLEDGMENTS

This work was supported in part by the US National Science Foundation under Grant No. PHY-0652548, PHY-0757839, PHY-0758115 and PHY-0457265, the Welch Foundation under Grant No. A-1358, the Research Corporation under Award No. 7123, the Texas Coordinating Board of Higher Education Award No. 003565-0004-2007, the National Natural Science Foundation of China under Grant Nos. 10575071, 10675082, 10874111, and 10647116, MOE of China under project NCET-05-0392, Shanghai Rising-Star Program under Grant No. 06QA14024, the SRF for ROCS, SEM of China, the National Basic Research Program of China (973 Program) under Contract No. 2007CB815004, and the Young Teachers' Training Program of the Chinese Scholarship Council under Grant No. 2007109651.

REFERENCES

1. B.A. Li, C.M. Ko and W. Bauer, Int. Jour. Mod. Phys. E **7**, 147 (1998).
2. Isospin Physics in Heavy-Ion Collisions at Intermediate Energies, Eds. Bao-An Li and W. Udo Schröder (Nova Science Publishers, Inc, New York, 2001).
3. P. Danielewicz, R. Lacey, W.G. Lynch, Science **298**, 1592 (2002).
4. V. Baran, M. Colonna, V. Greco and M. DiToro, Phys. Rep. **410**, 335 (2005).
5. B.A. Li, L.W. Chen and C.M. Ko, Phys. Rep. **464**, 113 (2008).
6. J.M. Lattimer and M. Prakash, Phys. Rep. **333-334**, 121 (2000); Astrophys. J. **550**, 426 (2001).
7. J.M. Lattimer and M. Prakash, Science **304**, 536 (2004).

8. J.M. Lattimer and M. Prakash, Phys. Rep. **442**, 109 (2007).
9. A.W. Steiner, M. Prakash, J.M. Lattimer, and P.J. Ellis, Phys. Rep. **410**, 325 (2005).
10. B.A. Li, C.B. Das, S. Das Gupta and C. Gale, Nucl. Phys. **A735**, 563 (2004); Phys. Rev. **C69**, 064602 (2004).
11. C. B. Das, S. Das Gupta, C. Gale and B.A. Li, Phys. Rev. **C67**, 034611 (2003).
12. C. Hartnack, Rajeev K. Puri, J. Aichelin, J. Konopka, S.A. Bass, H. Stoecker and W. Greiner, Euro. Phys. J., **A1**, 151 (1998).
13. A. Akmal, V.R. Pandharipande and D.G. Ravenhall, Phys. Rev. C 58 (1998) 1804.
14. M.B. Tsang et al., Phys. Rev. Lett. **92**, 062701 (2004).
15. L.W. Chen, C.M. Ko and B.A. Li Phys. Rev. Lett. **94**, 032701 (2005).
16. B.A. Li and L.W. Chen, Phys. Rev. **C72**, 064611 (2005).
17. L.W. Chen, C.M. Ko, and B.A. Li, Phys. Rev. C **72**, 064309 (2005).
18. M.B. Tsang et al., arXiv:0811.3107, Phys. Rev. Lett. (2009) in press.
19. Z.G. Xiao, B.A. Li, L.W.. Chen, G.C. Yong and M. Zhang, Phys. Rev. Lett. **102**, 062502 (2009).
20. W. Reisdorf et al., Nucl. Phys. A **781**, 459 (2007).
21. B.A. Li, Phys. Rev. Lett. **85**, 4221 (2000).
22. B.A. Li, Phys. Rev. Lett. **88**, 192701 (2002); Nucl. Phys. **A708**, 365 (2002).
23. M. Kutschera, Phys. Lett. **B340**, 1 (1994).
24. A. Szmaglinski et al., Acta Phys. Polon. **B37**, 277 (2006).
25. M. Kutschera et al., Phys. Rev. **C62**, 025802 (2000).
26. S. Banik and D. Bandyopadhyay, J. Phys. G **26**, 1495 (2000).
27. G. Baym, C. Pethick and P. Sutherland, Astrophys. J. **170**, 299 (1971).
28. G. Baym, H. A. Bethe and C. J. Pethick, Nucl. Phys. **A175**, 225 (1971).
29. C. J. Pethick and D. G. Ravenhall, Ann. Rev. Nucl. Part. Sci. **45**, 429 (1995).
30. C. J. Pethick, D. G. Ravenhall and C. P. Lorenz, Nucl. Phys. **A584**, 675 (1995).
31. B. Link, R. I. Epstein, J.M. Lattimer, Phys. Rev. Lett. **83**, 3362 (1999).
32. C.J. Horowitz et al., Phys. Rev. C **69**, 045804 (2004); C.J. Horowitz et al., Phys. Rev. C **70**, 065806 (2004)
33. A. Burrows, S. Reddy, and T. A. Thompson, Nucl. Phys. **A777**, 356 (2006).
34. B. J. Owen, Phys. Rev. Lett. **95** (2005) 211101.
35. S. B. Ruster, M. Hempel, and J. Schaffner-Bielich, Phys. Rev. C **73**, 035804 (2006).
36. J. Xu, L.W. Chen, B.A. Li, H.R. Ma, 2008, arXiv:0807.4477v1, Phys. Rev. C (2009) in press; arXiv:0901.2309v1 [astro-ph]
37. D.G. Ravenhall, C.J. Pethick, and J.R. Wilson, Phys. Rev. Lett. **50**, 2066 (1983).
38. K. Oyamatsu, Nucl. Phys. **A561**, 431 (1993).
39. A.W. Steiner, Phys. Rev. C **77**, 035805 (2008).
40. F. Douchin and P. Haensel, Phys. Lett. **B485**, 107 (2000).
41. F. Douchin and P. Haensel, A&A **380**, 151 (2001).
42. J. Carriere, C.J. Horowitz, and J. Piekarewicz, Astrophys. J. **593**, 463 (2003).
43. K. Oyamatsu and K. Iida, Phys. Rev. C **75**, 015801 (2007).
44. C. Ducoin, Ph. Chomaz and F. Gulminelli, Nucl. Phys. **A789**, 403 (2007).
45. S. Kubis, Phys. Rev. C **76**, 035801 (2007); Phys. Rev. C **70**, 065804 (2004).
46. A. Worley, P.G. Krastev and B.A. Li, Astrophys. J. **685**, 390 (2008).
47. C.J. Horowitz and J. Piekarewicz, Phys. Rev. Lett. **86**, 5647 (2001); Phys. Rev. C **64**, 062802 (R) (2001); Phys. Rev. C **66**, 055803 (2002).
48. J. Arponen, Nucl. Phys. **A191**, 257 (1972).
49. S.S. Avancini et al., 2008, arXiv:0812.3170v1 [nucl-th]
50. M. Maggiore, Nature **447** (2007) 651.
51. E. E. Flanagan and S. A. Hughes, New J. Phys. **7** (2005) 204.
52. B. Abbott *et al.* [LIGO Scientific Collaboration], Phys. Rev. Lett. **94** (2005) 181103; Phys. Rev. D **76** (2007) 042001.
53. F. Acernese *et al.*, Class. Quant. Grav. **24** (2007) S491.
54. P.G. Krastev, B.A. Li and A. Worley, Phys. Lett. **B668**, 1 (2008).
55. A. Worley, P.G. Krastev and B.A., Li, arXiv:0812.0408.
56. D.H. Wen, B.A. Li and P.G. Krastev, preprint (2009).
57. P.G. Krastev, B.A. Li and A. Worley, ApJ, **676**, 1170 (2008).
58. B. Haskell, N. Andersson, D. I. Jones, and L. Samuelsson, Phys. Rev. Lett. **99** (2007) 231101.
59. B. J. Owen, Phys. Rev. Lett. **95** (2005) 211101.
60. J. M. Lattimer and B. F. Schutz, Astrophys. J. **629** (2005) 979.
61. S. Chandrasekhar and V. Ferrari, Proc. R. Soc. London A **432**, 247(1991); *ibid*, **434**, 449(1991).
62. N. Andersson and K.D. Kokkotas,MNRAS, 299, 1059-1068 (1998).
63. O. Benhar, E. Berti and V. Ferrari, MNRAS **310**, 797(1999).
64. L.K. Tsui and P.T. Leung, MNRAS **357**, 1029(2005); Astrophys. J **631**, 495(2005).